tvst

Glaucoma

Reduced Aqueous Humor Outflow Pathway Arborization in Childhood Glaucoma Eyes

Shikha Gupta[1], Xiaowei Zhang[2], Arnav Panigrahi[1], Shakha[1], Raymond Fang[3], Clemens A. Strohmaier[2,4], Hao F. Zhang[3], Robert N. Weinreb[2], Viney Gupta[1], and Alex S. Huang[2]

[1] Dr. Rajendra Prasad Centre for Ophthalmic Sciences, All India Institute for Medical Sciences, New Delhi, India
[2] Hamilton Glaucoma Center, Viterbi Family Department of Ophthalmology, Shiley Eye Institute, University of California, San Diego, San Diego, CA, USA
[3] Department of Biomedical Engineering, Northwestern University, Evanston, IL, USA
[4] Department of Ophthalmology and Optometry, Kepler University Hospital, Johannes Kepler University, Linz, Austriav

Correspondence: Shikha Gupta, Glaucoma Services, Dr. Rajendra Prasad Center for Ophthalmic Sciences, All India Institute of Medical Sciences, Ansari Nagar, New Delhi 110029, India. e-mail: shikhagupta@aiims.edu

Received: October 19, 2023
Accepted: February 16, 2024
Published: March 27, 2024

Keywords: aqueous humor outflow; childhood glaucoma; aqueous angiography; ocular hypertension

Citation: Gupta S, Zhang X, Panigrahi A, Shakha, Fang R, Strohmaier CA, Zhang HF, Weinreb RN, Gupta V, Huang AS. Reduced aqueous humor outflow pathway arborization in childhood glaucoma eyes. Transl Vis Sci Technol. 2024;13(3):23, https://doi.org/10.1167/tvst.13.3.23

Purpose: To compare aqueous humor outflow (AHO) pathway patterns between eyes of childhood glaucoma patients and non-glaucomatous patients receiving cataract surgery.

Methods: Aqueous angiography was performed in childhood glaucoma eyes ($n = 5$) receiving glaucoma surgery and in pediatric ($n = 1$) and healthy adult ($n = 5$) eyes receiving cataract surgery. Indocyanine green (0.4%) was introduced into the anterior chamber, and AHO was imaged using an angiographic camera (SPECTRALIS HRA+OCT with Flex Module). Images were acquired and analyzed (ImageJ with Analyze Skeleton 2D/3D plugin) from the nasal sides of the eyes, the usual site of glaucoma angle procedures. Image analysis endpoints included AHO vessel length, maximum vessel length, number of branches, number of branch junctions, and vessel density.

Results: Qualitatively, childhood glaucoma eyes demonstrated lesser AHO pathway arborization compared to pediatric and adult eyes without glaucoma. Quantitatively, childhood glaucoma and healthy adult cataract eyes showed similar AHO pathway average branch lengths and maximum branch lengths ($P = 0.49$–0.99). However, childhood glaucoma eyes demonstrated fewer branches (childhood glaucoma, 198.2 ± 35.3; adult cataract, 506 ± 59.5; $P = 0.002$), fewer branch junctions (childhood glaucoma, 74.6 ± 13.9; adult cataract, 202 ± 41.2; $P = 0.019$), and lower vessel densities (childhood glaucoma, 8% ± 1.4%; adult cataract, 17% ± 2.5%; $P = 0.01$).

Conclusions: Childhood glaucoma patients demonstrated fewer distal AHO pathways and lesser AHO pathway arborization. These anatomical alternations may result in a new source of trabecular meshwork-independent AHO resistance in this disease cohort.

Translational Relevance: Elevated distal outflow pathway resistance due to decreased AHO pathway arborization may explain some cases of failed trabecular bypass surgery in childhood glaucoma.

Introduction

Glaucoma is a leading cause of vision loss worldwide[1]; however, this statement is mostly in reference to adulthood glaucoma. Childhood glaucoma is rarer, and less overall research has been performed to understand its unique pathophysiological features as well as to develop unique pediatric-specific treatments.[2,3]

Intraocular pressure (IOP) is the only modifiable glaucoma risk factor, and IOP lowering is the only U.S. Food and Drug Administration–approved glaucoma treatment.[4] Therefore, elevated IOP has been extensively studied in adult glaucoma. However, such

translational vision science & technology

studies are complicated by the fact that adults can have glaucoma without elevated mean IOP, referred to as normal- or low-tension glaucoma.[5] For this reason, IOP does not define glaucoma. In adults, glaucoma research is being performed to understand other IOP behaviors such as IOP fluctuation[6] or how optic neuropathy can arise independent of IOP. For the pediatric population, the relationship between eye pressure and glaucoma is less complex. Childhood glaucoma is believed to result from trabecular meshwork (TM) dysgenesis; hence, childhood glaucoma should be associated with abnormal aqueous humor outflow (AHO) resulting in elevated mean IOP, the key factor leading to optic nerve damage and vision loss. Thus, studying abnormal AHO may be more straightforward in childhood glaucoma eyes.

Aqueous angiography is a method that was developed to visualize AHO.[7] It originally started with the use of clinical tools readily available to perform intravenous vascular angiography (IVA) during standard-of-care management of patients with retinal vascular diseases.[8] For the anterior segment, these tools were brought into the laboratory and re-engineered for anterior segment AHO imaging. The same tracers used in IVA, such as fluorescein and indocyanine green (ICG), were introduced into the anterior chamber, and the AHO was imaged using an angiographic camera. These methods were initially developed in the laboratory using postmortem eyes[9,10] and then translated to live non-human primates,[12] healthy human volunteers,[13,14] and then glaucoma patients.[15] Results demonstrated that AHO is segmental. Postlimbal regions could demonstrate low- or high-flow AHO. AHO is also pulsatile and dynamic,[12,13] such that regions of high- or low-flow can decrease or increase across the eye. Both in eyes studied in the laboratory and in adult glaucoma patients, aqueous angiography showed that TM bypass surgery improved AHO patterns.[10,15] Current data may suggest that targeting baseline low-flow regions is more beneficial for IOP lowering.[16]

Here, we used aqueous angiography to demonstrate AHO patterns in pediatric eyes for the first time, to the best of our knowledge, and studied AHO in eyes with childhood glaucoma. We hypothesized that AHO pathways of childhood glaucoma eyes would demonstrate vascular abnormalities in comparison to eyes without glaucoma.

Methods

This study adhered to the tenets of the Declaration of Helsinki and was conducted after a research review by the Institutional Ethics Committee at the Dr. Rajendra Prasad Centre for Ophthalmic Sciences AIIMS in New Delhi, India (IEC-681/01/10.2021). Informed consent was acquired from the parents of pediatric subjects undergoing exam under anesthesia with glaucoma surgery ($n = 5$) or directly from adults undergoing cataract surgery ($n = 5$). Parents for one of the glaucoma cases above (that was unilateral) were additionally consented because of the presence of a unilateral cataract requiring surgery in the contralateral non-glaucomatous eye. Inclusion criteria for childhood glaucoma include enlarged corneal diameter (>12 mm) with baseline IOP > 22 mmHg detected before 3 years of age. Classification was based upon the Childhood Glaucoma Research Network classification system.[17]

Surgical Procedure

All subjects received anesthesia followed by surgical time-out, sterile prep, drape, and placement of a lid speculum. Children received intravenous sevoflurane for detailed exam under anesthesia followed by surgery. Cataract patients were dilated (1% tropicamide) prior to surgery. Then, a 1-mm side-port paracentesis was made slightly superior temporal (right eye) or inferotemporal (left eye) through which a Lewicky Anterior Chamber Maintainer (K20-3276, 20 g; Katena Products, Parsippany, NJ) was inserted. For all cases, aqueous humor was evacuated using a syringe followed by the addition of tracer (see following Aqueous Angiography section for details). After the aqueous angiography was completed, the Anterior Chamber Maintainer was removed, and ICG was irrigated from the anterior chamber using balanced salt solution (BSS). A 10-0 nylon suture was placed to secure the wound when glaucoma surgery was planned, and the surgical plan for both children and adults was proceeded with.

Aqueous Angiography

Aqueous angiography was performed similarly to what was previously described.[13,15] The surgical suite was arranged by moving the SPECTRALIS Flex Module (Heidelberg Engineering, Heidelberg, Germany) into the operating room. The SPECTRALIS Flex Module is a modified surgical boom arm that allows for stable three-dimensional manipulations and positioning of the SPECTRALIS HRA+OCT camera head relative to the patient's supine position and eye through the use of multiple pivot joints. Alignment of the angiographic images along the z-axis was controlled by an integrated

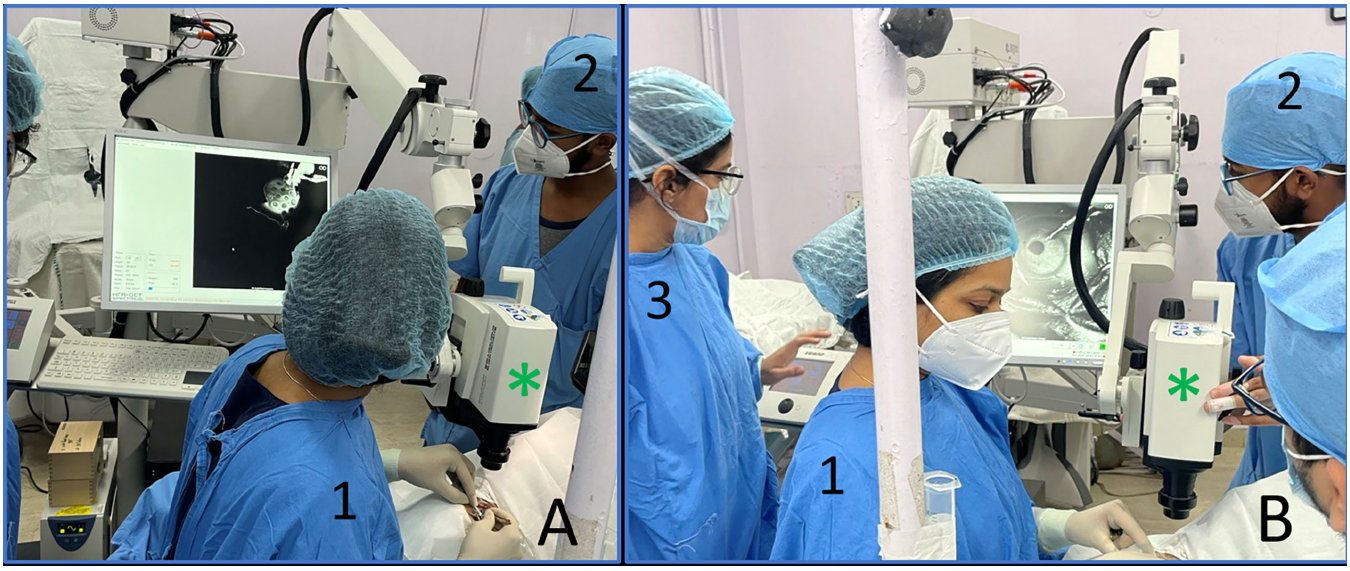

Figure 1. Imaging setup. (**A**) Surgeon view and (**B**) lateral view of aqueous angiography in the operating room. At least three individuals are required: (1) surgeon, (2) photographer, and (3) an individual to acquire the images using the software. *Green asterisks* indicate the camera head.

micromanipulator. The Flex Module was situated next to the patient's bed (Fig. 1). This provided a working space for the Flex Module operator at the side of the patient. Next to the head rest, an intravenous pole held a syringe reservoir with a three-way stopcock, situated ∼10 inches above the eye, which provided a gravity-delivered constant pressure of ∼18.7 mmHg.

From this position, the SPECTRALIS camera head was placed above the eye, and confocal scanning laser ophthalmoscopic infrared (IR) images were acquired to center the eye in the picture frame using a 30-degree lens with a 20-diopter focus. Subsequently, fluorescent images were obtained using ICG capture mode (excitation wavelength, 786 nm; transmission filter set at >800 nm) to establish a preinjection background that appeared black. Pharmaceutical-grade ICG (Aurogreen, ICG 25 mg; Aurolab, Kalikappan, India) was thoroughly dissolved with 0.7 mL of the manufacturer-provided solvent followed by 5.6 mL of BSS to a final 0.4% ICG concentration. These concentrations were chosen based on prior experience in postmortem eyes (cow[11] and human[10]) and in the eyes of living subjects (nonhuman primate[12] and human[13–15]). After introduction of the tracer, IR and angiographic images were acquired using the SPECTRALIS HRA+OCT Flex Module while grasping the eye and gently rotating it in different directions. The maximum time for allowable imaging was 3 minutes, and imaging was terminated if any tracer leak was observed on the ocular surface.

Image Analysis

Initial image review demonstrated variable image quality and degree of postlimbal exposure among different quadrants of the eye. Due to tracer handling, inadvertent staining of the ocular surface could make visualization poor. Thus, the only consistently imaged region was the nasal hemisphere. This made sense, as nasal imaging was easier due to temporal Anterior Chamber Maintainer placement. Further, because most angle-based surgeries are performed on the nasal hemisphere, it was decided to perform image analysis in the superior nasal, nasal, or inferior nasal parts of the eye. Quantitation for statistical analysis was performed only for childhood glaucoma and adult cataract eyes.

An examiner masked to the condition of the images performed the analysis using the ImageJ Fiji plugin (National Institutes of Health, Bethesda, MD) (Fig. 2). Scans with signal distortion due to insufficient focus or motion artifact leading to irregular vessel patterns were excluded. The portion of the original image (Fig. 2A) showing the cornea and underlying fluorescent signal from the anterior chamber was manually cropped (Fig. 2B), and the resultant image was binarized (Fig. 2C). A skeletonization algorithm was then applied (Fig. 2D), and the Analyze Skeleton 2D/3D algorithm[18,19] was used to quantify the number of branches, number of branch junctions, average branch length, and maximum branch length (Fig. 2E). Lengths were determined using built-in software with a scaling of 8.59 µm per pixel. For vessel density, the

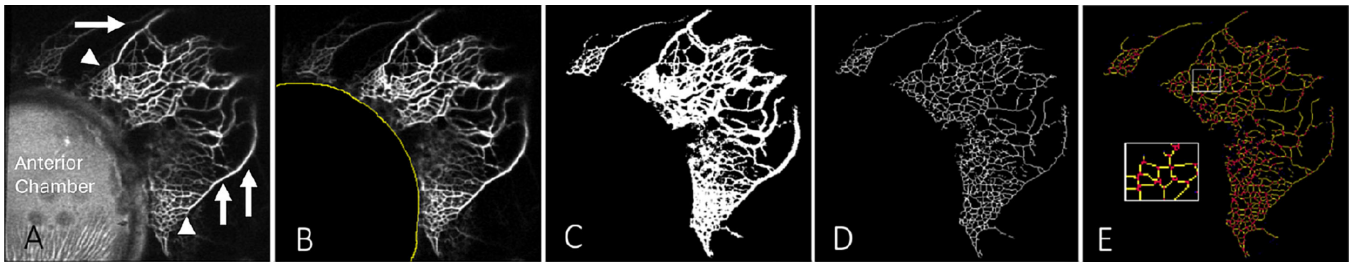

Figure 2. Image analysis. (**A**) Original image. (**B**) After segmentation or cropping of the cornea and anterior chamber; the *yellow curved line* denotes the limbus. (**C**) After binarization. (**D**) After skeletonization. (**E**) After Analyze Skeleton 2D/3D evaluation. *Yellow lines* are branches and *red dots* are junctions. Inset shows a zoomed-in region of interest. *Arrowheads* indicate intrascleral venous plexus, and *arrows* indicate aqueous or episcleral veins.

number of bright pixels in the cropped binarized image (Fig. 2C) was divided by the total pixel area of the same image outside the cropped region.

Circuit Analysis

A circuit analysis was performed on the skeletonized images to assess the contribution of vessel branching on theoretical AHO resistance in these eyes. Vessel width was not included in this analysis because vessel width within an image can be influenced by factors other than true vessel caliber, such as vessel depth, and aqueous angiography is not depth resolved. Based upon the average number of branches and junctions from aqueous angiography imaging, we generated electrical circuits to model fluid flow networks. We first generated 500 random graphs for each group where the number of nodes (N_N) and edges (N_E) were equal to the number of junctions and branches, respectively, using MATLAB 2023a (MathWorks, Natick, MA).[20] To generate the random graphs, we randomly selected two unconnected nodes following an even distribution between 1 and N_N and connected these two nodes with an edge. We repeated this process until the number of edges reached N_E and all nodes were connected to at least two other nodes. Then we generated a circuit by replacing each edge with a 1-ohm resistor. We applied 1-V voltage to the first node (N_1) and set the voltage of the last node (N_N) to 0 V. Using the simulated circuit, we applied Kirchhoff's laws to find the effective total conductance of the circuit.[21] Given that this analysis was only for the nasal quadrant (not intended to model the whole eye) and was only based on branches and junctions, the adult cataract eye conductance was arbitrarily set to an average value of 1 for relative comparison to childhood glaucoma eyes.

Data Analysis and Statistics

All data are presented as mean ± standard error of the mean (SEM). Comparisons between pediatric and adult eyes were performed using unpaired two-tailed *t*-tests (SigmaPlot 12.0; Inpixon, Palo Alto, CA).

Results

Aqueous angiography was performed in the eyes of childhood glaucoma patients ($n = 5$) and patients requiring cataract surgery (pediatric, $n = 1$; adult, $n = 5$) (Table). Among childhood glaucoma cases, the average age was 2.7 ± 1.6 years. Three were diagnosed with primary congenital glaucoma, and two were diagnosed with Axenfeld–Rieger syndrome. Among adults, the average age was 49.8 ± 5.8 years, and cataracts included nuclear sclerotic and posterior subcapsular types.

Aqueous angiography images on the nasal sides of the eyes were compared qualitatively. Imaging times after the start of aqueous angiography were similar across conditions: 107.2 ± 19.6 seconds for childhood glaucoma versus 110.2 ± 20.8 seconds for healthy adults ($P = 0.92$); the pediatric cataract time was 99 seconds. Aqueous angiography images normally capture distal outflow, past collector channels. Qualitatively, healthy adult eyes and the single pediatric cataract eye demonstrated expected patterns (Fig. 3). Additional images from the same location seconds apart from Figure 3 are shown in Supplementary Figure S1. Aqueous angiography showed the typical small branching intrascleral venous plexus and the normal larger Y-shaped aqueous and episcleral veins. Qualitative images from childhood glaucoma eyes also demonstrated expected Y-shaped branching, but the intrascleral venous plexus was less prominent with fewer overall vessels seen (Fig. 3)

Table. Subject Demographics

Subject	Age	Sex	Eye	Diagnosis	IOP (mmHg)	Corneal Diameter (mm)	CDR	Surgery	Imaging Time (s)
P1	5 mo	M	OS	PCG	35	14 × 14.5	0.8	GATT	68
P2	9 y	F	OD	ARS	30	13 × 13.5	0.9	TRAB	101
P3	1 y	M	OD	PCG	34	16 × 15	0.9	GATT	146
P4	11 mo	F	OD	ARS	31	13 × 13.5	0.7	TRAB	158
P5	2 y	M	OD	PCG	28	14.5 × 15	0.8	Goniotomy	63
PC	2 y	M	OD	Pediatric cataract	10	10.5 × 11	0.1	Cataract	99
A1	44 y	M	OD	Posterior subcapsular	XX	XX	XX	Cataract	157
A2	41 y	M	OS	Nuclear sclerosis	XX	XX	XX	Cataract	153
A3	40 y	M	OS	Nuclear sclerosis	XX	XX	XX	Cataract	68
A4	71 y	M	OD	Nuclear sclerosis	XX	XX	XX	Cataract	57
A5	53 y	F	OS	Nuclear sclerosis	XX	XX	XX	Cataract	116

IOP is the intraocular pressure of pediatric cases on presentation. Corneal diameter values are shown as vertical × horizontal. Imaging time is the imaging time used for image analysis. A, adult; ARS, Axenfeld–Rieger syndrome; CDR, cup-to-disc ratio; F, female; GATT, gonioscopy-assisted transluminal trabeculotomy; M, male; OD, right eye; OS, left eye; P, pediatric; PC, pediatric cataract case; PCG, primary congenital glaucoma; TRAB, trabeculotomy and trabeculectomy; XX, unavailable or irrelevant.

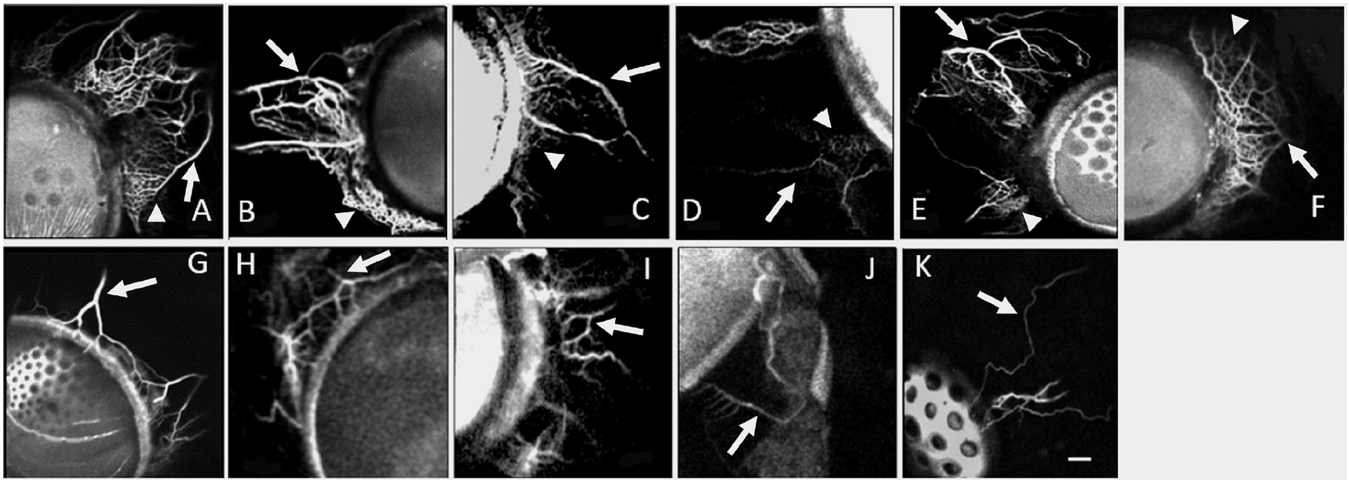

Figure 3. Aqueous angiography imaging. (**A**–**E**) Eyes from adult cataract patients. (**F**) Pediatric cataract case. (**G**–**K**) Eyes from childhood glaucoma patients. *Arrowheads* indicate intrascleral venous plexus, and *arrows* indicate aqueous or episcleral veins. *Scale bar*: 250 µm.

To quantitate outflow patterns, image analysis was performed. Similar to adult eyes, childhood glaucoma eyes showed comparable average branch length (childhood glaucoma, 88.7 ± 11.3 µm; adult cataract, 88.5 ± 8.0 µm; $P = 0.99$) and average maximum branch length (childhood glaucoma, 557.7 ± 126.4 µm; adult cataract, 444.2 ± 90.3 µm; $P = 0.49$) (Fig. 4). However, childhood glaucoma eyes demonstrated a reduced number of branches (childhood glaucoma, 198.2 ± 35.3 branches; adult cataract, 506 ± 59.5 branches; $P = 0.002$) and a reduced number of branch junctions (childhood glaucoma, 74.6 ± 13.9 junctions; adult cataract, 202 ± 41.2 junctions; $P = 0.019$) (Fig. 4). Childhood glaucoma eyes also demonstrated reduced vessel density (childhood glaucoma, 8% ± 1.4%; adult cataract, 17% ± 2.5%; $P = 0.01$) (Fig. 4). Data from the single congenital cataract case mirror adult results, but no statistical analyses were performed (average branch length, 142 µm; maximum branch length, 549 µm; branch number, 335 branches; branch junctions, 188 junctions; vessel density, 14%).

To estimate the impact of the observed decreased AHO pathway arborization in childhood glaucoma eyes, we estimated the relative change in AHO resistance arising from only distal outflow pathway data. Using only average branch and junction number data, 500 theoretical circuits were created each for childhood glaucoma and adult cataract eyes to model AHO circuits (Figs. 5A, 5B). In a relative comparison,

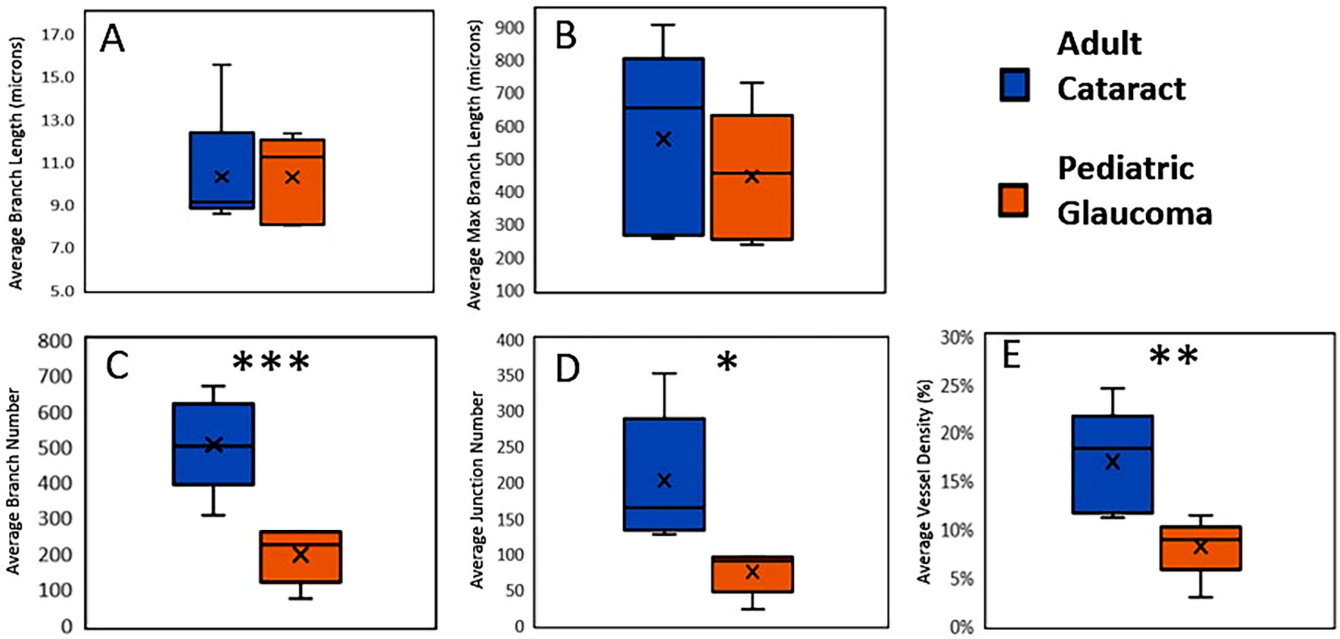

Figure 4. Quantitative distal AHO pathway assessment. Box-and-whisker plots. *X*, average; *center line*, median; *top of bar*, third quartile; *bottom of bar*, first quartile; *error bars*, maximum and minimum. $^{*}P < 0.05$; $^{**}P = 0.01$, $^{***}P < 0.01$.

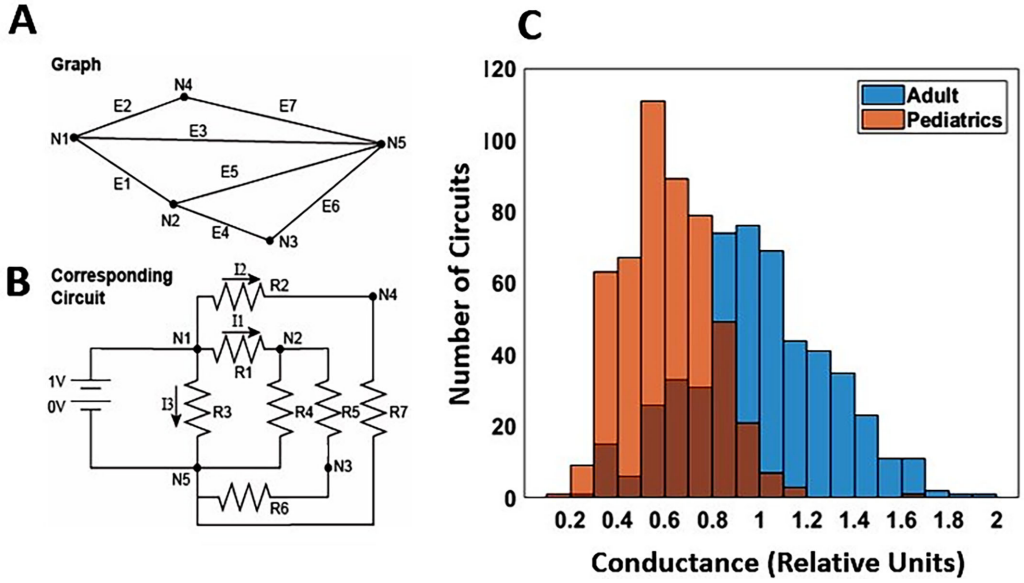

Figure 5. Circuit analysis. (**A**) An example graph with five nodes (N1–N5) and seven edges (E1–E7). (**B**) Circuit corresponding to graph in (**A**). The first node is connected to the input, and the last node (node 5 in this example) is connected to the ground. Edges in the graph correspond to resistors in the circuit (EX in graph corresponds to RX in circuit). The total current in the circuit corresponds to the sum of currents leaving the first node, which is the sum of I1 to I3 in this example. (**C**) Five hundred theoretical circuits were created each for childhood glaucoma and adult cataract eyes using the branch and junction data from Figure 4. The graphs corresponding to each circuit had nodes equal to the number of junctions and edges equal to the number of branches. Adult eyes were arbitrarily set to an average conductance value of 1 for relative comparison to childhood glaucoma eyes. *Blue* indicates adult; *orange*, pediatric; *dark orange*, overlap regions between *blue* and *orange*.

lower relative conductance (or increased resistance) was seen in the childhood glaucoma eyes (childhood glaucoma, 0.61 ± 0.01 relative conductance; adult cataract, 1.0 ± 0.13 relative conductance; $P < 0.001$) (Fig. 5C).

Discussion

We have shown for the first time, to the best of our knowledge, AHO patterns in pediatric eyes and

demonstrated altered AHO pathways in childhood glaucoma eyes using aqueous angiography. Viewed on the ocular surface, aqueous angiography directly visualizes distal outflow after aqueous humor leaves the TM and Schlemm's canal. Qualitatively and quantitatively, the results demonstrated that AHO branching was still present in the childhood glaucoma eyes with similar average branch length and average maximum branch length compared to non-glaucomatous eyes. Thus, existing AHO vessels in childhood glaucoma and non-glaucomatous eyes were similar. However, compared to adult eyes, childhood glaucoma eyes showed fewer branches, fewer branch junctions, and lower vessel density. In brief, childhood glaucoma eyes demonstrated decreased AHO pathway arborization.

Reduced AHO arborization may be relevant for elevated IOP. For all ages, the TM is known to be a major source of outflow resistance in the eye and the major source of elevated outflow resistance in ocular hypertension.[22] Segmental AHO is also associated with segmental regions of the TM showing locally increased or decreased AHO resistance.[23] Therefore, TM bypass or ablation is an effective surgery to lower IOP in adult and childhood glaucoma patients.[24,25] However, success is variable for unknown reasons. Recently, this has been a major limitation for adult TM-targeted minimally invasive glaucoma surgery, and this variability has stimulated considerable research into understanding adult AHO pathway physiology. In the childhood glaucoma eye, abnormal anatomy, such as a pre-TM Barkan's membrane[26] or abnormal primary TM development,[27] has been hypothesized and debated to be the cause of pathophysiological outflow resistance that can be alleviated by TM ablation. However, it is well known that both ab interno and ab externo trabeculotomies in childhood glaucoma eyes can still be ineffective for lowering IOP.[28] This suggests that, in both congenital and adult glaucoma eyes, resistance sources distal to the TM may be important.

The observation of decreased distal outflow arborization in childhood glaucoma eyes is consistent with potentially relevant distal AHO outflow resistance. Recall that, in an engineering circuit analysis, when resistors are placed in series, overall resistance in the circuit increases; however, when resistors are placed in parallel, overall resistance in the circuit decreases. Demonstrating decreased outflow pathway arborization in childhood glaucoma eyes is equivalent to saying that AHO outflow resistors are reduced in parallel. This may result in an additional TM-independent cause of elevated AHO resistance, which we have modeled (Fig. 5). Thus, the results from this work (1) potentially identify an additional source of post-TM outflow resistance in childhood glaucoma eyes and (2) may explain the failure of ab interno or ab externo trabeculotomy in some cases. What is unknown is whether distal AHO pathway changes are due to primary dysgenesis of the vessels or high IOP vessel collapse from lack of flow that subsequently could be rescued later. Critical to addressing this are planned studies using aqueous angiography after the initial glaucoma surgery at a later time to determine if rescue is possible and if that rescue correlates with IOP responses.

The comparison between childhood glaucoma patients and healthy adult volunteers warrants further discussion. Pediatric research is difficult to perform, and an appropriate comparator for a childhood glaucoma study is difficult to determine. The best control is simply a normal pediatric eye, but such eyes would never require surgery. Then, one could consider pediatric cataract eyes without glaucoma as a control. We show one case, but our group has limited research access to such patients as our division is responsible only for glaucoma, so we must rely on very rare unilateral glaucoma cases with contralateral cataracts. Also, it can be argued that pediatric cataract eyes are themselves fundamentally abnormal in the front of the eye. This is unlike adults, whose cataracts are considered a normal part of the aging process that just so happens to limit the patient's quality of life. Thus, for quantitation, we focused on comparing childhood glaucoma eyes to eyes from healthy adult volunteers requiring cataract surgery. This means that results could be influenced by differences in ocular development.

Another confounder between the adult cataract and childhood glaucoma cases relates to adult cataract surgery requiring pupil dilation using a muscarinic antagonist. Muscarinic activation is known to increase AHO.[29] Thus, in this case, the associated drug treatment would tend to decrease AHO in adult cataract eyes, leading to a theoretically diminished difference between the two groups. However, statistically significant differences were still seen, suggesting that the underlying differences between childhood glaucoma and adult cataract eyes could be greater.

Genetics must also be considered. For primary congenital glaucoma, *CYP1B1* mutations[30] represent the main genetic cause of childhood glaucoma. However, *TEK* mutations,[31,32] exist as well, with current research suggesting that *TEK* mutations impact distal AHO pathways. As childhood glaucoma is likely more heterogeneous than we appreciate, the type of genetic mutation may influence the source of AHO resistance, as well. In this study, the genetic mutations are not known, and this can be further studied in the future.

There are additional limitations of this study. First, the sample size is small because childhood glaucoma is relatively rare and research participation is less. Also, ocular surface staining from the tracers precluded a more comprehensive evaluation of circumferential outflow patterns around the limbus. Thus, a tracer-free method to study AHO pathways is preferable. Recent work in human eyes studying segmental TM pigmentation did not show that variable segmental TM pigmentation matched segmental AHO patterns.[33] Another option is anterior segment optical coherence tomography (AS-OCT). Although it has been used to study AHO pathways,[34,35] additional technological development is first needed for further study. Most AS-OCTs are simply posterior segment OCTs adapted for the anterior segment. An AHO-specific AS-OCT needs to be developed (including features of tracking/averaging with proper wavelength and angle of illumination). AHO-specific AS-OCT would allow better research to be performed, including non-invasive circumferential imaging around the limbus and potentially defining the relationship between the AHO pathway structure and outflow patterns to allow structural assessment alone to be sufficient in describing AHO.

In conclusion, childhood glaucoma eyes demonstrated visible distal AHO pathways with the use of aqueous angiography, but they showed less arborization. This could be due to childhood glaucoma changes in AHO pathways and may represent an additional source of post-TM AHO resistance that is unaccounted for by angle surgery.

Acknowledgments

Supported by grants from the National Institutes of Health (R01EY030501 to ASH, U01EY033001 to HFZ, F30EY034033 to RF), by a Research to Prevent Blindness Career Advancement Award CAA (AH), by an unrestricted grant from Research to Prevent Blindness, and by a Roche/ARVO Collaborative Research Fellowship Award (SG). The sponsors or funding organizations had no role in the design or conduct of this research.

Disclosure: **S. Gupta**, None; **X. Zhang**, None; **A. Panigrahi**, None; **Shakha**, None; **R. Fang**, None; **C.A. Strohmaier**, AbbVie (R), Elios Vision (C, R), Santen Pharmaceutical (C, F), Zeiss (R); **H.F. Zhang**, Opticent Health (F), **R.N. Weinreb**, Alcon (C), Allergan (C), Amydis (C, F), Editas (C), Equinox Ophthalmic (C), Iantrek (C), iSTAR Medical (C), Santen (C), Topcon (C); **V. Gupta**, None; **A.S. Huang**, Allergan (C), Amydis (C), Celanese (C), Diagnosys (F), Equinox Ophthalmic (C), Glaukos (C, F), Heidelberg Engineering (F), QLARIS (C), Santen (C), Topcon (C)

References

1. Weinreb RN, Khaw PT. Primary open-angle glaucoma. *Lancet*. 2004;363(9422):1711–1720.
2. Papadopoulos M, Vanner EA, Grajewski AL, International study of childhood glaucoma–childhood glaucoma research network study group. International Study of Childhood Glaucoma. *Ophthalmol Glaucoma*. 2020;3(2):145–157.
3. Giangiacomo A, Beck A. Pediatric glaucoma: review of recent literature. *Curr Opin Ophthalmol*. 2017;28(2):199–203.
4. Musch DC, Gillespie BW, Niziol LM, Lichter PR, Varma R, CIGTS Study Group. Intraocular pressure control and long-term visual field loss in the collaborative initial glaucoma treatment study. *Ophthalmology*. 2011;118(9):1766–1773.
5. Collaborative Normal-Tension Glaucoma Study Group. The effectiveness of intraocular pressure reduction in the treatment of normal-tension glaucoma. *Am J Ophthalmol*. 1998;126(4):498–505.
6. Kim JH, Caprioli J. Intraocular pressure fluctuation: is it important? *J Ophthalmic Vis Res*. 2018;13(2):170–174.
7. Lee JY, Akiyama G, Saraswathy S, et al. Aqueous humour outflow imaging: seeing is believing. *Eye (Lond)*. 2021;35(1):202–215.
8. Keane PA, Sadda SR. Imaging chorioretinal vascular disease. *Eye (Lond)*. 2010;24(3):422–427.
9. Saraswathy S, Tan JC, Yu F, et al. Aqueous angiography: real-time and physiologic aqueous humor outflow imaging. *PLoS One*. 2016;11(1):e0147176.
10. Huang AS, Saraswathy S, Dastiridou A, et al. Aqueous angiography-mediated guidance of trabecular bypass improves angiographic outflow in human enucleated eyes. *Invest Ophthalmol Vis Sci.* 2016;57(11):4558–4565, doi:10.1167/iovs.16-19644.
11. Huang AS, Saraswathy S, Dastiridou A, et al. Aqueous angiography with fluorescein and indocyanine green in bovine eyes. *Transl Vis Sci Technol.* 2016;5(6):5, doi:10.1167/tvst.5.6.5.
12. Huang AS, Li M, Yang D, Wang H, Wang N, Weinreb RN. Aqueous angiography in living nonhuman primates shows segmental, pulsatile, and dynamic angiographic aqueous humor outflow. *Ophthalmology*. 2017;124(6):793–803.

13. Huang AS, Camp A, Xu BY, Penteado RC, Weinreb RN. Aqueous angiography: aqueous humor outflow imaging in live human subjects. *Ophthalmology*. 2017;124(8):1249–1251.
14. Huang AS, Penteado RC, Saha SK, et al. Fluorescein aqueous angiography in live normal human eyes. *J Glaucoma*. 2018;27(11):957–964.
15. Huang AS, Penteado RC, Papoyan V, Voskanyan L, Weinreb RN. Aqueous angiographic outflow improvement after trabecular microbypass in glaucoma patients. *Ophthalmol Glaucoma*. 2019;2(1):11–21.
16. Strohmaier CA, Wanderer D, Zhang X, et al. Greater outflow facility increase after targeted trabecular bypass in angiographically determined low-flow regions. *Ophthalmol Glaucoma*. 2023;6(6):570–579.
17. Thau A, Lloyd M, Freedman S, Beck A, Grajewski A, Levin AV. New classification system for pediatric glaucoma: implications for clinical care and a research registry. *Curr Opin Ophthalmol*. 2018;29(5):385–394.
18. Flavel RJ, Guppy CN, Rabbi SMR, Young IM. An image processing and analysis tool for identifying and analysing complex plant root systems in 3D soil using non-destructive analysis: Root1. *PLoS One*. 2017;12(5):e0176433.
19. Srinivasan A, Muñoz-Estrada J, Bourgeois JR, et al. BranchAnalysis2D/3D automates morphometry analyses of branching structures. *J Neurosci Methods*. 2018;294:1–6.
20. Dorfler F, Simpson-Porco J, Bullo F. Electrical networks and algebraic graph theory: models, properties, and applications. *Proc IEEE*. 2018; 106(5):977–1005.
21. Urbano M. *Introductory Electrical Engineering with Math Explained in Accessible Language*. New York: John Wiley & Sons; 2019.
22. Johnson M. What controls aqueous humour outflow resistance?. *Exp Eye Res*. 2006;82(4):545–557.
23. Strohmaier CA, McDonnell FS, Zhang X, et al. Differences in outflow facility between angiographically identified high- versus low-flow regions of the conventional outflow pathways in porcine eyes. *Invest Ophthalmol Vis Sci*. 2023;64(3):29.
24. Dorairaj SK, Seibold LK, Radcliffe NM, et al. 12-Month outcomes of goniotomy performed using the Kahook Dual Blade combined with cataract surgery in eyes with medically treated glaucoma. *Adv Ther*. 2018;35(9):1460–1469.
25. Morales J, Al Shahwan S, Al Odhayb S, Al Jadaan I, Edward DP. Current surgical options for the management of pediatric glaucoma. *J Ophthalmol*. 2013;2013:763735.
26. Barkan O. Pathogenesis of congenital glaucoma: gonioscopic and anatomic observation of the angle of the anterior chamber in the normal eye and in congenital glaucoma. *Am J Ophthalmol*. 1955;40(1):1–11.
27. Anderson DR. The development of the trabecular meshwork and its abnormality in primary infantile glaucoma. *Trans Am Ophthalmol Soc*. 1981;79:458–485.
28. El Sayed Y, Esmael A, Mettias N, El Sanabary Z, Gawdat G. Factors influencing the outcome of goniotomy and trabeculotomy in primary congenital glaucoma. *Br J Ophthalmol*. 2021;105(9):1250–1255.
29. Naveh-Floman N, Stahl V, Korczyn AD. Effect of pilocarpine on intraocular pressure in ocular hypertensive subjects. *Ophthalmic Res*. 1986;18(1):34–37.
30. Lewis CJ, Hedberg-Buenz A, DeLuca AP, Stone EM, Alward WLM, Fingert JH. Primary congenital and developmental glaucomas. *Hum Mol Genet*. 2017;26(R1):R28–R36.
31. Souma T, Tompson SW, Thomson BR, et al. Angiopoietin receptor TEK mutations underlie primary congenital glaucoma with variable expressivity. *J Clin Invest*. 2016;126(7):2575–2587.
32. Thomson BR, Souma T, Tompson SW, et al. Angiopoietin-1 is required for Schlemm's canal development in mice and humans. *J Clin Invest*. 2017;127(12):4421–4436.
33. Strohmaier CA, Wanderer D, Zhang X, et al. Lack of correlation between segmental trabecular meshwork pigmentation and angiographically determined outflow in ex-vivo human eyes [published online ahead of print October 5, 2023]. *J Glaucoma*, https://doi.org/10.1097/IJG.0000000000002318.
34. Huang AS, Belghith A, Dastiridou A, Chopra V, Zangwill LM, Weinreb RN. Automated circumferential construction of first-order aqueous humor outflow pathways using spectral-domain optical coherence tomography. *J Biomed Opt*. 2017;22(6):66010.
35. Kagemann L, Wollstein G, Ishikawa H, et al. Visualization of the conventional outflow pathway in the living human eye. *Ophthalmology*. 2012;119(8):1563–1568.